DISCRETE AND CONTINUOUS
DYNAMICAL SYSTEMS SERIES B

doi:10.3934/dcdsb.2020262

EFFICIENT AND ACCURATE SAV SCHEMES FOR THE GENERALIZED ZAKHAROV SYSTEMS

Jie Shen

Department of Mathematics, Purdue University
West Lafayette, IN 47907, USA

Nan Zheng

School of Mathematical Sciences
Fujian Provincial Key Laboratory of Mathematical Modeling
and High-Performance Scientific Computing
Xiamen University, Xiamen 361005, China

Abstract. We develop in this paper efficient and accurate numerical schemes based on the scalar auxiliary variable (SAV) approach for the generalized Zakharov system and generalized vector Zakharov system. These schemes are second-order in time, linear, unconditionally stable, only require solving linear systems with constant coefficients at each time step, and preserve exactly a modified Hamiltonian. Ample numerical results are presented to demonstrate the accuracy and robustness of the schemes.

1. **Introduction.** We consider in this paper numerical approximations of the generalized and vector Zakharov systems using the scalar auxiliary variable (SAV) approach.

The generalized Zakharov system (GZS) [10, 9] describes the propagation of Langmuir waves in plasma. It takes the following form

$$\begin{cases} i\partial_t E + \triangle E - \alpha N E + \lambda |E|^2 E = 0, \\ N_t = -\nabla \cdot \mathbf{V}, \\ \mathbf{V}_t = -\dfrac{1}{\epsilon^2}\nabla(N - \nu|E|^2), \end{cases} \qquad (x,t) \in \Omega \times (0, +\infty), \tag{1.1}$$

with initial conditions

$$E(x,0) = E_0(x), \quad N(x,0) = N_0(x), \quad N_t(x,0) = N_1(x), \quad x \in \Omega, \tag{1.2}$$

where $\Omega = \mathbb{R}^d$ $(d = 1, 2, 3)$ with zero boundary conditions at infinities, or $\Omega = (-L, L)^d$ $(d = 1, 2, 3)$ with periodic boundary conditions. In the above, E is a complex function represents the slowly varying envelope of the highly oscillatory electric field, N is a real function describing the deviation of the ion density from its equilibrium value, ϵ is a parameter inversely proportional to the acoustic speed, $\alpha > 0$, λ, ν are real parameters. In the special case $\epsilon = 1$, $\lambda = 0$, $\nu = -1$, it reduces to the classical Zakharov system derived in [19] to model the collapse of caverns.

2020 *Mathematics Subject Classification.* 35Q55, 65M12, 65M70.

Key words and phrases. generalized Zakharov system, scalar auxiliary variable, Hamiltonian system, stability.

This work is partially supported by NSF grant DMS-1720442 and NSFC grant 11971407.

The GZS conserves the wave energy, momentum and Hamiltonian defined by:

$$\begin{aligned} D &= \int_\Omega |E(\mathbf{x},t)|^2 d\mathbf{x}, \\ \mathbf{P} &= \int_\Omega \frac{i}{2}(E\nabla\overline{E} - \overline{E}\nabla E) - \frac{\epsilon^2\alpha}{\nu} N\mathbf{V} d\mathbf{x}, \\ H &= \int_\Omega |\nabla E|^2 + \alpha N|E|^2 - \frac{\lambda}{2}|E|^4 - \frac{\alpha}{2\nu}N^2 - \frac{\alpha\epsilon^2}{2\nu}|\mathbf{V}|^2 d\mathbf{x}. \end{aligned} \tag{1.3}$$

On the other hand, the generalized vector Zakarov system(GVZS) [4] takes the form

$$\begin{cases} i\partial_t \mathbf{E} + a\triangle\mathbf{E} + (1-a)\nabla(\nabla\cdot\mathbf{E}) - \alpha N\mathbf{E} + \lambda|\mathbf{E}|^2\mathbf{E} = 0, \\ N_t = -\nabla\cdot\mathbf{V}, \\ \mathbf{V}_t = -\dfrac{1}{\epsilon^2}\nabla(N - \nu|\mathbf{E}|^2), \end{cases} \quad (x,t)\in\Omega\times(0,+\infty), \tag{1.4}$$

with initial conditions

$$\mathbf{E}(x,0) = \mathbf{E}_0(x), \quad N(x,0) = N_0(x), \quad N_t(x,0) = N_1(x), \quad x\in\Omega, \tag{1.5}$$

where same Ω and boundary conditions as for VGS in (1.1). In the above, the complex vector function $\mathbf{E}$ is still the slowly varying envelope of the highly oscillatory electric field, and the real function N is the deviation of the ion density from its equilibrium value, a, $\alpha > 0$ and λ are real parameters. In the special case $\lambda = 0$, $\alpha = 1$, it reduces to the standard vector Zakharov system (VGS) considered in [17].

The GVZS also conserves the wave energy, momentum and Hamiltonian defined by:

$$\begin{aligned} D &= \int_\Omega |\mathbf{E}(\mathbf{x},t)|^2 d\mathbf{x}, \\ \mathbf{P} &= \int_\Omega \frac{i}{2}\sum_{j=1}^{d}(E_j\nabla\overline{E_j} - \overline{E_j}\nabla E_j) - \frac{\epsilon^2\alpha}{\nu} N\mathbf{V} d\mathbf{x}, \\ H &= \int_\Omega a|\nabla\mathbf{E}|^2 + (1-a)|\nabla\cdot\mathbf{E}|^2 + \alpha N|\mathbf{E}|^2 \\ &\quad - \frac{\lambda}{2}|\mathbf{E}|^4 - \frac{\alpha}{2\nu}N^2 - \frac{\alpha\epsilon^2}{2\nu}|\mathbf{V}|^2 d\mathbf{x}. \end{aligned} \tag{1.6}$$

There have been various attempts in designing efficient numerical schemes for GZS an VGZS, e.g., finite difference methods [8, 7], the Fourier pseudospectral methods [12, 13], wavelet-Galerkin methods [1], discrete singular convolution method [18], time-splitting spectral discretizations [4] and time-splitting multiscale time integrator [3], among others. It is relatively easy to construct numerical schemes which preserve the wave energy, but it is very difficult for a numerical scheme to preserve the Hamiltonian and momentum.

Recently, the so called scalar auxiliary variable (SAV) approach was proposed in [15, 16] for gradient flows. The SAV approach can leading to numerical schemes which are unconditionally energy stable for gradient flows. It can also be used to construct efficient numerical schemes preserving the Hamiltonian structures [6, 2]. In this paper, we shall use the SAV approach to construct efficient numerical time

discretization schemes for the GZS and VGZS. These schemes enjoy the following advantages:

- it is second-order accurate in time and unconditionally stable;
- it only requires solving linear differential equations with constant coefficients at each time step;
- it preserves exactly a modified Hamiltonian, and preserves the original Hamiltonian and wave energy with third-order accuracy and the momentum with second-order accuracy.

These schemes can be coupled with any consistent Galerkin type spatial discretization in space, e.g., with the Fourier-spectral method, it only involves inverting diagonal linear systems, so they are very efficient and flexible.

The rest of the paper is organized as follows. In Section 2, we describe the semi-discrete Crank-Nicolson SAV scheme for the VGS, and use the Fourier-spectral method in space, as an example, to construct a fully discretized scheme for VGS with periodic boundary conditions. In Section 3, we construct the semi-discrete Crank-Nicolson SAV schemes for the GVZS. In Section 4, we present some numerical results using the Fourier-spectral SAV schemes for the GZS and GVZS with periodic boundary conditions. Some concluding remarks are given in the final section.

2. SAV schemes for GZS.

In this section, we first construct a SAV scheme for GZS based on the semi-implicit Crank-Nicolson Adam-Bashforth method. Then, we consider the periodic boundary condition and use a Fourier-spectral method in space to construct a fully discretized scheme.

2.1. Semi-discrete in time.

Since the Hamiltonian defined in (1.3) is conserved, we have that

$$\int_\Omega -\alpha N|E|^2+\frac{\lambda}{2}|E|^4 d\mathbf{x}=\int_\Omega |\nabla E|^2-\frac{\alpha}{2\nu}N^2-\frac{\alpha\epsilon^2}{2\nu}|\mathbf{V}|^2 d\mathbf{x}-H|_{t=0}.$$

Thus, in the usual cases where $\alpha/\nu<0$, we can choose $C_0>0$ such that

$$\int_\Omega -\alpha N|E|^2+\frac{\lambda}{2}|E|^4 d\mathbf{x}\geq -H|_{t=0}>-C_0. \tag{2.1}$$

Note that the above is true with (E,N) being a solution of (1.1). Since numerical solutions constructed below are expected to converge to the exact solution, we can reasonably assume that if we choose C_0 sufficiently large, (2.1) would also hold for any convergent numerical solution. Therefore, we can introduce a SAV defined by

$$r(t)=\sqrt{\int_\Omega \alpha N|E|^2-\frac{\lambda}{2}|E|^4 d\mathbf{x}+C_0}, \tag{2.2}$$

and rewrite the system (1.1) as

$$i\partial_t E=-\triangle E+r(t)W_1(E,N), \tag{2.3a}$$

$$N_t=-\nabla\cdot\mathbf{V}, \tag{2.3b}$$

$$\mathbf{V}_t=-\frac{1}{\epsilon^2}\nabla(N-\frac{2\nu}{\alpha}r(t)W_2(E,N)), \tag{2.3c}$$

$$r_t=\int_\Omega Re(W_1(E,N)\overline{E_t})+W_2(E,N)N_t d\mathbf{x}. \tag{2.3d}$$

where

$$W_1(E,N) := \frac{\delta r}{\delta \overline{E}} = \frac{\alpha N E - \lambda |E|^2 E}{\sqrt{\int_\Omega \alpha N|E|^2 - \frac{\lambda}{2}|E|^4 d\mathbf{x} + C_0}},$$
$$W_2(E,N) := \frac{\delta r}{\delta N} = \frac{\alpha |E|^2}{2\sqrt{\int_\Omega \alpha N|E|^2 - \frac{\lambda}{2}|E|^4 d\mathbf{x} + C_0}}. \tag{2.4}$$

If we set $r(0) = \sqrt{\int_\Omega \alpha N|E|^2 - \frac{\lambda}{2}|E|^4 d\mathbf{x} + C_0}|_{t=0}$, then the above system is exactly the same as the original GZS (1.1). In particular, it preserves the Hamiltonian in the sense that

$$\frac{d}{dt}(\|\nabla E\|^2 + r^2 - \frac{\alpha}{2\nu}\|N\|^2 - \frac{\alpha\epsilon^2}{2\nu}\|\mathbf{V}\|^2) = 0. \tag{2.5}$$

Indeed, taking the L^2 inner products of (2.3a) with $\overline{E_t}$, of (2.3b) with $\frac{\alpha}{2\nu}N$,of (2.3c) with $\frac{\alpha\epsilon^2}{2\nu}\mathbf{V}$ and of (2.3d) with $-r(t)$, summing up the real parts of these relations, we obtain immediately (2.5).

We construct below a SAV scheme based on the Crank-Nicolson Adam-Bashforth method for the system (2.3).

A semi-discrete scheme for GZS. Assuming E^n, E^{n-1}, N^n, N^{n-1}, $\mathbf{V}^n$, $\mathbf{V}^{n-1}$ and r^n, $r^{n-1}$are known, we update E^{n+1}, N^{n+1}, $\mathbf{V}^{n+1}$ and r^{n+1} as follows:

$$i\frac{E^{n+1}-E^n}{dt} = -\triangle E^{n+\frac{1}{2}} + r^{n+\frac{1}{2}} W_1(E^{\star,n+\frac{1}{2}}, N^{\star,n+\frac{1}{2}}), \tag{2.6a}$$

$$\frac{N^{n+1}-N^n}{dt} = -\nabla\cdot\mathbf{V}^{n+\frac{1}{2}}, \tag{2.6b}$$

$$\frac{\mathbf{V}^{n+1}-\mathbf{V}^n}{dt} = -\frac{1}{\epsilon^2}\nabla N^{n+\frac{1}{2}} + \frac{2\nu}{\alpha\epsilon^2} r^{n+\frac{1}{2}}\nabla W_2(E^{\star,n+\frac{1}{2}}, N^{\star,n+\frac{1}{2}}), \tag{2.6c}$$

$$\begin{aligned}\frac{r^{n+1}-r^n}{dt} = &\int_\Omega Re(W_1(E^{\star,n+\frac{1}{2}}, N^{\star,n+\frac{1}{2}})\frac{\overline{E^{n+1}}-\overline{E^n}}{dt}) \\ &+ W_2(E^{\star,n+\frac{1}{2}}, N^{\star,n+\frac{1}{2}})\frac{N^{n+1}-N^n}{dt}d\mathbf{x}.\end{aligned} \tag{2.6d}$$

where, for any sequence of functions $\{F^k\}$, $F^{n+\frac{1}{2}} = \frac{1}{2}(F^{n+1}+F^n)$, $F^{\star,n+\frac{1}{2}} = \frac{3}{2}F^n - \frac{1}{2}F^{n-1}$.

Before we discuss how to solve the above coupled system, we first establish the following result.

Theorem 2.1. *The scheme (2.6) unconditionally preserves a modified Hamiltonian in the sense that*

$$\begin{aligned}&\|\nabla E^{n+1}\|^2 + (r^{n+1})^2 - \frac{\alpha}{2\nu}\|N^{n+1}\|^2 - \frac{\alpha\epsilon^2}{2\nu}\|\boldsymbol{V}^{n+1}\|^2 \\ =&\|\nabla E^n\|^2 + (r^n)^2 - \frac{\alpha}{2\nu}\|N^n\|^2 - \frac{\alpha\epsilon^2}{2\nu}\|\boldsymbol{V}^n\|^2.\end{aligned} \tag{2.7}$$

Furthermore, the scheme (2.6) admits a unique solution if $\frac{\alpha}{\nu} < 0$.

Proof. We first prove (2.7). Taking the L^2 inner products of (2.6a) with $\frac{\overline{E^{n+1}}-\overline{E^n}}{dt}$, of (2.6b) with $\frac{\alpha}{2\nu}N^{n+\frac{1}{2}}$, of (2.6c) with $\frac{\alpha\epsilon^2}{2\nu}\mathbf{V}^{n+\frac{1}{2}}$, and multiplying (2.6d) with $-r^{n+\frac{1}{2}}$, summing up the real parts of these relations, one obtains immediately (2.7).

Thanks to (2.7), the system (2.6) has at most one solution if $\frac{\alpha}{\nu} < 0$ (with suitable boundary conditions on E). Since (2.6) is a linear system for $(E^{n+1}, N^{n+1}, \mathbf{V}^{n+1}, r^{n+1})$, we conclude that the scheme (2.6) admits a unique solution if $\frac{\alpha}{\nu} < 0$. □

We now describe how to efficiently implement the scheme (2.6). Note that E^{n+1} and N^{n+1} ($\mathbf{V}^{n+1}$ is just an intermediate variable which can be eliminated) in the system (2.6) is coupled by a scalar r^{n+1}. Hence, the coupled system can be decoupled by using a block-Gaussian elimination process. For the readers' convenience, we provide an explicit procedure below.

From (2.6d), we have:

$$\begin{aligned} r^{n+1} =& r^n + \int_\Omega Re(W_1(E^{\star,n+\frac{1}{2}}, N^{\star,n+\frac{1}{2}})\overline{E^{n+1}} - W_1(E^{\star,n+\frac{1}{2}}, N^{\star,n+\frac{1}{2}})\overline{E^n}) \\ &+ W_2(E^{\star,n+\frac{1}{2}}, N^{\star,n+\frac{1}{2}})N^{n+1} - W_2(E^{\star,n+\frac{1}{2}}, N^{\star,n+\frac{1}{2}})N^n d\mathbf{x}. \end{aligned} \tag{2.8}$$

To simplify the notations, we denote

$$\beta = Re(W_1(E^{\star,n+\frac{1}{2}}, N^{\star,n+\frac{1}{2}}), \overline{E^{n+1}}) + (W_2(E^{\star,n+\frac{1}{2}}, N^{\star,n+\frac{1}{2}}), N^{n+1}).$$

Plugging the above into (2.6a) and (2.6c), we can eliminate r^{n+1} from (2.6) to obtain

$$(\frac{1}{2}\triangle + \frac{i}{dt})E^{n+1} - \frac{1}{2}\beta W_1(E^{\star,n+\frac{1}{2}}, N^{\star,n+\frac{1}{2}}) = g_1^{n+\frac{1}{2}}, \tag{2.9a}$$

$$(\frac{1}{dt} - \frac{dt}{4\epsilon^2}\triangle)N^{n+1} + \frac{\nu dt}{2\alpha\epsilon^2}\beta\triangle W_2(E^{\star,n+\frac{1}{2}}, N^{\star,n+\frac{1}{2}}) = g_2^{n+\frac{1}{2}}, \tag{2.9b}$$

where

$$\begin{aligned} g_1^{n+\frac{1}{2}} =& (\frac{i}{dt} - \frac{1}{2}\triangle)E^n + r^n W_1(E^{\star,n+\frac{1}{2}}, N^{\star,n+\frac{1}{2}}) \\ &- \frac{1}{2}\beta W_1(E^{\star,n+\frac{1}{2}}, N^{\star,n+\frac{1}{2}}), \end{aligned}$$

$$\begin{aligned} g_2^{n+\frac{1}{2}} =& (\frac{1}{dt} + \frac{dt}{4\epsilon^2}\triangle)N^n - \nabla\cdot\mathbf{V}^n - \frac{\nu dt}{\alpha\epsilon^2}r^n\triangle W_2(E^{\star,n+\frac{1}{2}}, N^{\star,n+\frac{1}{2}}) \\ &+ \frac{\nu dt}{2\alpha\epsilon^2}\beta\triangle W_2(E^{\star,n+\frac{1}{2}}, N^{\star,n+\frac{1}{2}}), \end{aligned}$$

and

$$\nabla\cdot\mathbf{V}^n = -\frac{2}{dt}N^n + \frac{2}{dt}N^{n-1} - \nabla\cdot\mathbf{V}^{n-1}.$$

Writing

$$E^{n+1} = E_0^{n+1} + \beta E_1^{n+1}, \tag{2.10a}$$

$$N^{n+1} = N_0^{n+1} + \beta N_1^{n+1}, \tag{2.10b}$$

in (2.9), we obtain the following four decoupled equations:

$$(\frac{1}{2}\triangle + \frac{i}{dt})E_0^{n+1} = g_1^{n+\frac{1}{2}}, \tag{2.11a}$$

$$(\frac{1}{2}\triangle + \frac{i}{dt})E_1^{n+1} = \frac{1}{2}W_1(E^{\star,n+\frac{1}{2}}, N^{\star,n+\frac{1}{2}}), \tag{2.11b}$$

$$(\frac{1}{dt} - \frac{dt}{4\epsilon^2}\triangle)N_0^{n+1} = g_2^{n+\frac{1}{2}}, \tag{2.11c}$$

$$(\frac{1}{dt} - \frac{dt}{4\epsilon^2}\triangle)N_1^{n+1} = -\frac{\nu dt}{2\alpha\epsilon^2}\triangle W_2(E^{\star,n+\frac{1}{2}}, N^{\star,n+\frac{1}{2}}), \tag{2.11d}$$

with the same boundary conditions for the exact solutions (E, N).

It remains to determine β. To this end, taking the inner products of (2.10a) with $W_1(E^{\star,n+\frac{1}{2}}, N^{\star,n+\frac{1}{2}})$, or of (2.10b) with $W_2(E^{\star,n+\frac{1}{2}}, N^{\star,n+\frac{1}{2}})$, summing up their real parts, we obtain

$$\Big[1 - Re(W_1(E^{\star,n+\frac{1}{2}}, N^{\star,n+\frac{1}{2}}), \overline{E_1^{n+1}})\Big]\,\beta = Re(W_1(E^{\star,n+\frac{1}{2}}, N^{\star,n+\frac{1}{2}}), \overline{E_0^{n+1}}), \tag{2.12}$$

from which β can be determined.

To summarize, we can obtain E^{n+1}, N^{n+1}, $\mathbf{V}^{n+1}$ and r^{n+1} from (2.6) as follows:

1. Solve $(E_i^{n+1}, N_i^{n+1},\ i = 0, 1)$ from (2.11);
2. Determine β from (2.12);
3. Obtain E^{n+1}, N^{n+1} from (2.10), then determine $\mathbf{V}^{n+1}$ and r^{n+1} from (2.6c)-(2.6d).

Thus, the main computational cost is to solve the four decoupled linear systems with constant coefficients in (2.11) which can be efficiently solved with your favorite numerical method.

2.2. **Full discretization with a Fourier-spectral method in space.** As in [4], we shall restrict ourselves to the space periodic case, namely we take $\Omega = [0, 2\pi)^d$ for the sake of simplicity, and use the Fourier-spectral method [5, 14] in space to construct a fully discrete version of the scheme (2.6).

We shall describe our scheme in the three-dimensional case only as one- and two-dimensional cases can be dealt with similarly. Let us denote

$$X_M = \text{span}\{e^{ikx}e^{ipy}e^{iqz} : -\frac{M}{2} \le k, p, q \le \frac{M}{2} - 1\}.$$

Then, any function $E(\mathbf{x}, t) \in X_M$ can be expanded as

$$E(\mathbf{x}, t) = \sum_{k=-M/2}^{M/2-1} \sum_{p=-M/2}^{M/2-1} \sum_{q=-M/2}^{M/2-1} \hat{E}_{k,p,q}(t) e^{ikx} e^{ipy} e^{iqz}. \tag{2.13}$$

Based on the above results, we can construct the full-discrete second-order Crank-Nicolson Fourier-spectral scheme for the system (2.6).

A fully discretized SAV scheme for GZS. Given E_M^n, E_M^{n-1}, N_M^n, N_M^{n-1}, $\mathbf{V}_M^n$, $\mathbf{V}_M^{n-1}$ and R^n, R^{n-1}, we compute E_M^{n+1}, N_M^{n+1}, $\mathbf{V}_M^{n+1}$ and R^{n+1} by solving

$$(i\frac{E_M^{n+1} - E_M^n}{dt}, \psi) = (\nabla E_M^{n+\frac{1}{2}}, \nabla\psi) + (R^{n+\frac{1}{2}} W_1(E_M^{\star,n+\frac{1}{2}}, N_M^{\star,n+\frac{1}{2}}), \psi), \quad \forall \psi \in X_M, \tag{2.14a}$$

$$(\frac{N_M^{n+1} - N_M^n}{dt}, \sigma) = -(\nabla \cdot \mathbf{V}_M^{n+\frac{1}{2}}, \sigma), \quad \forall \sigma \in X_M, \tag{2.14b}$$

$$\begin{aligned}(\frac{\mathbf{V}_M^{n+1} - \mathbf{V}_M^n}{dt}, \zeta) = &-\frac{1}{\epsilon^2}(\nabla N_M^{n+\frac{1}{2}}, \zeta) \\ &+ \frac{2\nu}{\alpha\epsilon^2}(R^{n+\frac{1}{2}} \nabla W_2(E_M^{\star,n+\frac{1}{2}}, N_M^{\star,n+\frac{1}{2}}), \zeta), \quad \forall \zeta \in X_M,\end{aligned} \tag{2.14c}$$

$$\begin{aligned}\frac{R^{n+1} - R^n}{dt} = &\int_\Omega Re(W_1(E_M^{\star,n+\frac{1}{2}}, N_M^{\star,n+\frac{1}{2}}) \frac{\overline{E_M^{n+1}} - \overline{E_M^n}}{dt}) \\ &+ W_2(E_M^{\star,n+\frac{1}{2}}, N_M^{\star,n+\frac{1}{2}}) \frac{N_M^{n+1} - N_M^n}{dt} d\mathbf{x},\end{aligned} \tag{2.14d}$$

where $E_M^0 = \Pi_M E_0$, $N_M^0 = \Pi_M N_0$, $E_M^{\star,n+\frac{1}{2}} = \frac{3}{2}E_M^n - \frac{1}{2}E_M^{n-1}$, $N_M^{\star,n+\frac{1}{2}} = \frac{3}{2}N_M^n - \frac{1}{2}N_M^{n-1}$, and Π_M is the orthogonal projection operator from $L^2(\Omega)$ onto X_M.

By using exactly the same arguments as in the proof of Theorem 2.1, we can establish the following result:

Theorem 2.2. *The scheme (2.14) unconditionally preserves a discrete Hamiltonian in the sense that*

$$\begin{aligned}&\|\nabla E_M^{n+1}\|^2 + (R^{n+1})^2 - \frac{\alpha}{2\nu}\|N_M^{n+1}\|^2 - \frac{\alpha\epsilon^2}{2\nu}\|\boldsymbol{V}_M^{n+1}\|^2\\ =&\|\nabla E_M^n\|^2 + (R^n)^2 - \frac{\alpha}{2\nu}\|N_M^n\|^2 - \frac{\alpha\epsilon^2}{2\nu}\|\boldsymbol{V}_M^n\|^2.\end{aligned} \tag{2.15}$$

Furthermore, the scheme (2.14) admits a unique solution if $\frac{\alpha}{\nu} < 0$.

The efficient implementation procedure for the scheme (2.6) outlined above applies directly to the scheme (2.6). In particular, the main computational cost is to solve the discrete versions of the four decoupled equations in (2.11). In the case of periodic boundary conditions, the Fourier-spectral approximation of these decoupled equations leads to diagonal systems in the Fourier frequency space so that they can solved very efficiently.

3. The SAV schemes for the GVZS.

Similarly as for the GZS, we can construct efficient SAV schemes for the GVZS (1.4). As for the GZS, the GVZS also conserves the Hamiltonian H defined in (1.6). Therefore,

$$\int_\Omega -\alpha N|\mathbf{E}|^2 + \frac{\lambda}{2}|\mathbf{E}|^4 d\mathbf{x} = \int_\Omega a|\nabla\mathbf{E}|^2 + (1-a)|\nabla\cdot\mathbf{E}|^2 - \frac{\alpha}{2\nu}N^2 - \frac{\alpha\epsilon^2}{2\nu}|\mathbf{V}|^2 d\mathbf{x} - H|_{t=0}.$$

Hence, in the usual cases where $a > 0$ and $\alpha/\nu < 0$, we can also choose $C_0 > 0$ such that

$$\int_\Omega -\alpha N|\mathbf{E}|^2 + \frac{\lambda}{2}|\mathbf{E}|^4 d\mathbf{x} \geq -H|_{t=0} > -C_0. \tag{3.1}$$

Introducing the following SAV:

$$r(t) = \sqrt{\int_\Omega \alpha N|\mathbf{E}|^2 - \frac{\lambda}{2}|\mathbf{E}|^4 d\mathbf{x} + C_0}, \tag{3.2}$$

we can rewrite the system (1.4) as:

$$i\partial_t\mathbf{E} = -a\triangle\mathbf{E} - (1-a)\nabla\nabla\cdot\mathbf{E} + r(t)\mathbf{W}_1(\mathbf{E},N), \tag{3.3a}$$

$$N_t = -\nabla\cdot\mathbf{V}, \tag{3.3b}$$

$$\mathbf{V}_t = -\frac{1}{\epsilon^2}\nabla(N - \frac{2\nu}{\alpha}r(t)W_2(\mathbf{E},N)) \tag{3.3c}$$

$$r_t = \int_\Omega \sum_{j=1}^d Re(W_{1j}(\mathbf{E},N)\frac{\delta\overline{E}_j}{\delta t}) + W_2(\mathbf{E},N)\frac{\delta N}{\delta t}d\mathbf{x}, \tag{3.3d}$$

where $\mathbf{W}_1(\mathbf{E},N) = (W_{11}, W_{12}, W_{13})$ with

$$W_{1j}(\mathbf{E},N) = \frac{\delta r}{\delta\overline{E}_j} = \frac{\alpha N E_j - \lambda|\mathbf{E}|^2 E_j}{\sqrt{\int_\Omega \alpha N|\mathbf{E}|^2 - \frac{\lambda}{2}|\mathbf{E}|^4 d\mathbf{x} + C_0}}, \tag{3.4}$$

and

$$W_2(\mathbf{E},N) = \frac{\delta r}{\delta N} = \frac{\alpha|\mathbf{E}|^2}{2\sqrt{\int_\Omega \alpha N|\mathbf{E}|^2 - \frac{\lambda}{2}|\mathbf{E}|^4 d\mathbf{x} + C_0}}. \tag{3.5}$$

If we set $r(0)=\sqrt{\int_\Omega \alpha N|\mathbf{E}|^2-\frac{\lambda}{2}|\mathbf{E}|^4 d\mathbf{x}+C_0}|_{t=0}$, the system (3.3) is exactly equivalent to (1.4). In particular, it preserves the Hamiltonian in the sense that

$$\frac{d}{dt}(a\|\nabla\mathbf{E}\|^2+(1-a)\|\nabla\cdot\mathbf{E}\|^2+r^2-\frac{\alpha}{2\nu}\|N\|^2-\frac{\alpha\epsilon^2}{2\nu}\|\mathbf{V}\|^2)=0. \tag{3.6}$$

Indeed, taking the L^2 inner products of (3.3a) with $\frac{\delta\overline{\mathbf{E}}}{\delta t}$, of (3.3b) with $\frac{\alpha}{2\nu}N$, of (3.3c) with $\frac{\alpha\epsilon^2}{2\nu}\mathbf{V}$, and multiplying (3.3d) with $-r(t)$, summing up the real parts of theses relations, we arrive at (3.6).

We now construct a semi-discrete in time scheme for the system (3.3):

The SAV scheme for the GVZS. Assuming $\mathbf{E}^n$, $\mathbf{E}^{n-1}$, N^n, N^{n-1}, $\mathbf{V}^n$, $\mathbf{V}^{n-1}$ and r^n, r^{n-1} are known, we update $\mathbf{E}^{n+1}$, N^{n+1}, $\mathbf{V}^{n+1}$ and r^{n+1} by solving

$$i\frac{\mathbf{E}^{n+1}-\mathbf{E}^n}{dt}=-a\triangle\mathbf{E}^{n+\frac12}-(1-a)\nabla\nabla\cdot\mathbf{E}^{n+\frac12}+r^{n+\frac12}\mathbf{W}_1(\mathbf{E}^{\star,n+\frac12},N^{\star,n+\frac12}), \tag{3.7a}$$

$$\frac{N^{n+1}-N^n}{dt}=-\nabla\cdot\mathbf{V}^{n+\frac12}, \tag{3.7b}$$

$$\frac{\mathbf{V}^{n+1}-\mathbf{V}^n}{dt}=-\frac{1}{\epsilon^2}\nabla N^{n+\frac12}+\frac{2\nu}{\alpha\epsilon^2}r^{n+\frac12}\nabla W_2(\mathbf{E}^{\star,n+\frac12},N^{\star,n+\frac12}), \tag{3.7c}$$

$$\begin{aligned}\frac{r^{n+1}-r^n}{dt}=&\int_\Omega\sum_{k=1}^3 Re(W_{1k}(\mathbf{E}^{\star,n+\frac12},N^{\star,n+\frac12})\frac{\overline{E_k^{n+1}}-\overline{E_k^n}}{dt})\\&+W_2(\mathbf{E}^{\star,n+\frac12},N^{\star,n+\frac12})\frac{N^{n+1}-N^n}{dt}d\mathbf{x}.\end{aligned} \tag{3.7d}$$

Theorem 3.1. *The scheme (3.7) unconditionally preserves a modified Hamiltonian in the sense that*

$$\begin{aligned}&a\|\nabla\boldsymbol{E}^{n+1}\|^2+(1-a)\|\nabla\cdot\boldsymbol{E}^{n+1}\|^2+(r^{n+1})^2-\frac{\alpha}{2\nu}\|N^{n+1}\|^2-\frac{\alpha\epsilon^2}{2\nu}\|\boldsymbol{V}^{n+1}\|^2\\=&a\|\nabla\boldsymbol{E}^{n}\|^2+(1-a)\|\nabla\cdot\boldsymbol{E}^{n}\|^2+(r^{n})^2-\frac{\alpha}{2\nu}\|N^{n}\|^2-\frac{\alpha\epsilon^2}{2\nu}\|\boldsymbol{V}^{n}\|^2.\end{aligned} \tag{3.8}$$

Furthermore, the scheme (3.7) admits a unique solution if $a>0$ and $\frac{\alpha}{\nu}<0$.

Proof. Taking the inner products of (3.7a) with $\frac{\overline{\mathbf{E}^{n+1}}-\overline{\mathbf{E}^n}}{dt}$, of (3.7b) with $\frac{\alpha}{2\nu}N^{n+\frac12}$, of (3.7c) with $\frac{\alpha\epsilon^2}{2\nu}\mathbf{V}^{n+\frac12}$ and multiplying (3.7d) with $-r^{n+\frac12}$, summing up the real parts, one obtains (3.8) immediately.

Since $\Delta\mathbf{E}=\nabla\nabla\cdot\mathbf{E}-\nabla\times\nabla\times\mathbf{E}$, one can check that $\|\nabla\cdot\mathbf{E}\|^2\le\|\nabla\mathbf{E}\|^2$ for any $\mathbf{E}\in H_0^1(\Omega)$ or $H_p^1(\Omega)=\{\mathbf{E}\in H^1(\Omega):\mathbf{E}\text{ periodic}\}$. Hence, if $a>0$ and $\frac{\alpha}{\nu}<0$, we find that the modified Hamiltonian in the left and right sides of (3.8) are non-negative. Therefore, we derive from (3.8) immediately that solution of (3.7) must be unique. Since the scheme (3.7) is linear, we conclude that it admits a unique solution. □

We now describe how to solve (3.7) efficiently. To simplify the notations, we denote

$$\beta=\sum_{k=1}^3 Re(W_{1k}(\mathbf{E}^{\star,n+\frac12},N^{\star,n+\frac12}),\overline{E_k^{n+1}})+(W_2(\mathbf{E}^{\star,n+\frac12},N^{\star,n+\frac12}),N^{n+1}).$$

First, we can eliminate r^{n+1} from (3.7) to obtain

$$\begin{aligned}&(\frac{a}{2}\triangle+\frac{i}{dt})\mathbf{E}^{n+1}+\frac{(1-a)}{2}\nabla\nabla\cdot\mathbf{E}^{n+1}\\&-\frac{1}{2}\beta\mathbf{W}_1(\mathbf{E}^{\star,n+\frac{1}{2}},N^{\star,n+\frac{1}{2}})=\mathbf{g}_1^{n+\frac{1}{2}},\end{aligned}\tag{3.9a}$$

$$(\frac{1}{dt}-\frac{dt}{4\epsilon^2}\triangle)N^{n+1}+\frac{\nu dt}{2\alpha\epsilon^2}\beta\triangle W_2(\mathbf{E}^{\star,n+\frac{1}{2}},N^{\star,n+\frac{1}{2}})=g_2^{n+\frac{1}{2}},\tag{3.9b}$$

where $\mathbf{g}_1^{n+\frac{1}{2}}$ and $g_2^{n+\frac{1}{2}}$ contain all terms depending on previous time steps, given by

$$\begin{aligned}\mathbf{g}_1^{n+\frac{1}{2}}=&(\frac{i}{dt}-\frac{a}{2}\triangle)\mathbf{E}^n-\frac{(1-a)}{2}\nabla\nabla\cdot\mathbf{E}^n+r^n\mathbf{W}_1(\mathbf{E}^{\star,n+\frac{1}{2}},N^{\star,n+\frac{1}{2}})\\&-\frac{1}{2}\beta\mathbf{W}_1(\mathbf{E}^{\star,n+\frac{1}{2}},N^{\star,n+\frac{1}{2}}),\\g_2^{n+\frac{1}{2}}=&(\frac{1}{dt}+\frac{dt}{4\epsilon^2}\triangle)N^n-\nabla\cdot\mathbf{V}^n-\frac{\nu dt}{\alpha\epsilon^2}r^n\triangle W_2(\mathbf{E}^{\star,n+\frac{1}{2}},N^{\star,n+\frac{1}{2}})\\&+\frac{\nu dt}{2\alpha\epsilon^2}\beta\triangle W_2(\mathbf{E}^{\star,n+\frac{1}{2}},N^{\star,n+\frac{1}{2}}).\end{aligned}$$

Writing

$$\mathbf{E}^{n+1}=\mathbf{E}_0^{n+1}+\beta\mathbf{E}_1^{n+1},\tag{3.10a}$$

$$N^{n+1}=N_0^{n+1}+\beta N_1^{n+1}\tag{3.10b}$$

in (3.9), we obtain the following four decoupled equations

$$(\frac{a}{2}\triangle+\frac{i}{dt})\mathbf{E}_0^{n+1}+\frac{(1-a)}{2}\nabla\nabla\cdot\mathbf{E}_0^{n+1}=\mathbf{g}_1^{n+\frac{1}{2}},\tag{3.11a}$$

$$(\frac{a}{2}\triangle+\frac{i}{dt})\mathbf{E}_1^{n+1}+\frac{(1-a)}{2}\nabla\nabla\cdot\mathbf{E}_1^{n+1}=\frac{1}{2}\mathbf{W}_1(\mathbf{E}^{\star,n+\frac{1}{2}},N^{\star,n+\frac{1}{2}}),\tag{3.11b}$$

$$(\frac{1}{dt}-\frac{dt}{4\epsilon^2}\triangle)N_0^{n+1}=g_2^{n+\frac{1}{2}},\tag{3.11c}$$

$$(\frac{1}{dt}-\frac{dt}{4\epsilon^2}\triangle)N_1^{n+1}=-\frac{\nu dt}{2\alpha\epsilon^2}\triangle W_2(\mathbf{E}^{\star,n+\frac{1}{2}},N^{\star,n+\frac{1}{2}}).\tag{3.11d}$$

It remains to determine β. To this end, we take the inner products of (3.10a) with $\mathbf{W}_1(\mathbf{E}^{\star,n+\frac{1}{2}},N^{\star,n+\frac{1}{2}})$, or of (3.10b) with $W_2(\mathbf{E}^{\star,n+\frac{1}{2}},N^{\star,n+\frac{1}{2}})$, summing up their real parts, we obtain

$$\left[1-\sum_{k=1}^{3}Re(W_{1k}(\mathbf{E}^{\star,n+\frac{1}{2}},N^{\star,n+\frac{1}{2}}),\overline{E_{1k}^{n+1}})\right]\beta=\sum_{k=1}^{3}Re(W_{1k}(\mathbf{E}^{\star,n+\frac{1}{2}},N^{\star,n+\frac{1}{2}}),\overline{E_{0k}^{n+1}}),\tag{3.12}$$

from which we can determine β.

In summary, we can obtain $\mathbf{E}^{n+1}$, N^{n+1}, $\mathbf{V}^{n+1}$ and r^{n+1} from (3.7) as follows:

1. Solve $(\mathbf{E}_i^{n+1},N_i^{n+1},\ i=0,1)$ from (3.11);
2. Determine β from (3.12);
3. Obtain $\mathbf{E}^{n+1}$, N^{n+1} from (3.10), and $\mathbf{V}^{n+1}$ and r^{n+1} from (3.7c)-(3.7d).

Thus, the main computational cost is to solve the four decoupled linear systems with constant coefficients in (3.11) which can be efficiently solved with your favorite numerical method.

As in the case for GZS, the main computational cost is to solve the four decoupled linear systems with constant coefficients in (3.11) which can be efficiently solved with your favorite numerical method. In particular, in the case of periodic boundary

conditions that we consider in this paper, a Fourier-spectral method applied to (3.11c)-(3.11d) still leads to diagonal systems that can be efficiently solved, however, the two components of $\mathbf{E}_i^{n+1}$ are coupled in (3.11a)-(3.11b). We now describe how to efficiently solve (3.11a)-(3.11b) with the Fourier-spectral method. Since the linear system for (3.11b) is exactly the same as for (3.11a), we shall only consider (3.11a). We first expand the unknown $\mathbf{E}_0$ and the righ hand side function $\mathbf{g}_1^{n+\frac{1}{2}}$ in Fourier series

$$(\mathbf{E}_0, \mathbf{g}_1^{n+\frac{1}{2}}) = \sum_{k=-M/2}^{M/2-1} \sum_{p=-M/2}^{M/2-1} \sum_{q=-M/2}^{M/2-1} (\hat{\mathbf{E}}_{kpq}, \hat{\mathbf{g}}_{kpq}) e^{ikx} e^{ipy} e^{iqz}. \tag{3.13}$$

Plugging the above into (3.11a), we obtain, for each (k,p,q), the following 3×3 system for the unknowns $\hat{\mathbf{E}}_{kpq} = (\widehat{E}^1_{kpq}, \widehat{E}^2_{kpq}, \widehat{E}^3_{kpq})^t$:

$$A_{kpq} \begin{pmatrix} \widehat{E}^1_{kpq} \\ \widehat{E}^2_{kpq} \\ \widehat{E}^3_{kpq} \end{pmatrix} = \widehat{\mathbf{g}}_{kqp}, \tag{3.14}$$

with

$$A_{kpq} = \begin{pmatrix} -\frac{a}{2}(p^2+q^2) - \frac{1}{2}k^2 + \frac{i}{dt} & -\frac{1-a}{2}kp & -\frac{1-a}{2}kq \\ -\frac{1-a}{2}kp & -\frac{a}{2}(k^2+q^2) - \frac{1}{2}p^2 + \frac{i}{dt} & -\frac{1-a}{2}pq \\ -\frac{1-a}{2}kq & -\frac{1-a}{2}pq & -\frac{a}{2}(k^2+p^2) - \frac{1}{2}q^2 + \frac{i}{dt} \end{pmatrix}. \tag{3.15}$$

It can be checked that for $a > 0$ and all (k, p, q), we have

$$\begin{aligned} &det(A_{kpq}) \\ &= \left(-\frac{a}{2}(k^2+p^2+q^2) + \frac{i}{dt}\right) \cdot \left(\frac{a}{4}(k^2+p^2+q^2)^2 - \frac{(a+1)i}{2dt}(k^2+p^2+q^2) - \frac{1}{dt^2}\right) \neq 0. \end{aligned} \tag{3.16}$$

Hence, the system (3.14) admits a unique solution. Therefore, (3.11a), as well as (3.11b), can be solved efficiently.

4. Numerical simulations.

In this section, we present some numerical results using the Fourier-spectral SAV schemes for the GZS and GVZS with periodic boundary conditions. Unless otherwise specified, we take $C_0 = 10$ which is sufficient to ensure $\{r^k\}$ well defined in most cases except the simulation of blowup.

4.1. The standard ZS with a solitary-wave solution.

The classical Zakharov system (ZS), (1.1) with $\epsilon = 1$, $\lambda = 0$, $\nu = -1$, admits a solitary-wave solution given by [11, 9]:

$$\begin{aligned} E(x,t) &= \sqrt{2B^2(1-\epsilon^2C^2)}\,\mathrm{sech}(B(x-Ct))e^{i[(C/2)x-((C/2)^2-B^2)t]}, \\ N(x,t) &= -2B^2\mathrm{sech}^2(B(x-Ct)). \end{aligned} \tag{4.1}$$

where B,C are constants. In this test, we choose $d = 1$ and $\alpha = 1$ in (1.1). The initial condition is taken as

$$E^{(0)}(x) = E(x,0), \quad N^{(0)}(x) = N(x,0), \quad N^{(1)}(x) = \partial_t N(x,0). \tag{4.2}$$

We set $e_E = E_{exact} - E_{approx.}$, $e_N = N_{exact} - N_{approx.}$, and similarly $e_I^{GZS} = I_{exact}^{GZS} - I_{approx.}^{GZS}$ for $I = D, P, H$. We present below numerical results for three cases with different regimes of the acoustic speed.

Case I. *O(1)-acoustic speed regime*, i.e., $\epsilon = 1$, we choose $B = 1$, $C = 0.5$ in (4.1). The computational domain is $\Omega = [-32, 32)$, and we computed for time up to

$T = 1$. We first use 256 Fourier modes to discretize the space variable so that the spatial discretization error can be ignored compared with time discretization error. In Table 1, we list the errors for various time steps. The results clearly show that second-order accuracy is achieved.

TABLE 1. Error and convergence rates in time.

δt	$\lvert e_E\rvert_{L^\infty(0,T;L^\infty)}$	*Rate*	$\lvert e_N\rvert_{L^\infty(0,T;L^\infty)}$	*Rate*
2×10^{-2}	1.90E(-3)	–	1.60E(-3)	–
1×10^{-2}	4.82E(-4)	1.98	3.94E(-4)	1.98
5×10^{-3}	1.21E(-4)	1.99	9.93E(-5)	1.99
2.5×10^{-3}	3.04E(-5)	2.00	2.49E(-5)	2.00
1.25×10^{-3}	7.61E(-6)	2.00	6.23E(-6)	2.00
6.25×10^{-4}	1.90E(-6)	2.00	1.56E(-6)	2.00
3.125×10^{-4}	4.76E(-7)	2.00	3.93E(-7)	1.99
1.5625×10^{-4}	1.21E(-7)	1.97	1.08E(-7)	1.87

Next, we examine the discretization error in space [14]. We take $dt = 10^{-5}$ so that the time discretization is negligeable compared with the spatial discretization error. From Table 2, we observe that the spatial errors converge exponentially.

TABLE 2. Discretization Error in space.

N	32	64	128	256
$\lvert e_E\rvert_{L^\infty(0,T;L^\infty)}$	5.40E(-1)	7.84E(-2)	1.91E(-4)	8.88E(-7)
$\lvert e_N\rvert_{L^\infty(0,T;L^\infty)}$	2.64E(-1)	1.23E(-1)	1.10E(-3)	5.19E(-6)

While it is clear that the Crank-Nicolson SAV schemes are second-order accurate for the unknown functions and preserve the modified Hamiltonian exactly, it is not clear how the conserved quantities would be preserved. We observe from Table 3 that the wave energy D and original Hamiltonian H are preserved with third-order accuracy while the momentum P is preserved with second-order accuracy.

TABLE 3. Error and convergence rates for the conserved quantities.

δt	$\lvert e_{DGZS}\rvert_{L^\infty(0,T)}$	*Rate*	$\lvert e_P^{GZS}\rvert_{L^\infty(0,T)}$	*Rate*	$\lvert e_H^{GZS}\rvert_{L^\infty(0,T)}$	*Rate*
8×10^{-2}	1.50E(-3)	–	2.10E(-3)	–	2.00E(-3)	–
4×10^{-2}	1.69E(-4)	3.14	4.68E(-4)	2.16	2.26E(-4)	3.10
2×10^{-2}	2.05E(-5)	3.04	1.12E(-4)	2.07	2.90E(-5)	3.02
1×10^{-2}	2.53E(-6)	3.02	2.73E(-5)	2.03	3.60E(-6)	3.01
5×10^{-3}	3.14E(-7)	3.01	6.74E(-6)	2.02	4.49E(-7)	3.00
2.5×10^{-3}	3.91E(-8)	3.01	1.68E(-6)	2.01	5.61E(-8)	3.00
1.25×10^{-3}	4.88E(-9)	3.00	4.18E(-7)	2.00	7.09E(-9)	2.98
6.25×10^{-4}	6.09E(-10)	3.00	1.05E(-7)	1.99	1.18E(-9)	2.58

Case II. *"Subsonic limit" regime*, i.e., $0 \le \epsilon \ll 1$. We take B=1 and $C = 1/2\epsilon$, so the wavelength of the initial data (4.1) is $O(\epsilon)$. Here we take $\Omega = (-32, 32)$ with 128 Fourier modes, and test the ϵ-resolution of different time steps.

Figures 4.1 and 4.2 indicate that for different ϵ, $dt = 10^{-3}$ and $dt = 10^{-1}$ lead to indistinguishable numerical results.

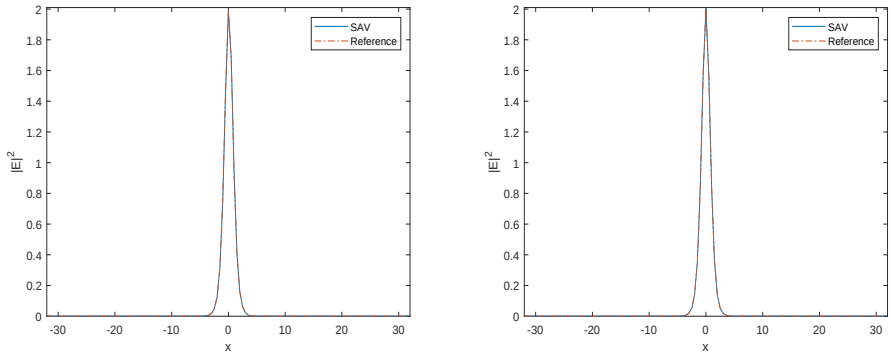

(a) $\epsilon = 0.125, dt = 10^{-3}$ (b) $\epsilon = 0.125/16, dt = 10^{-3}$

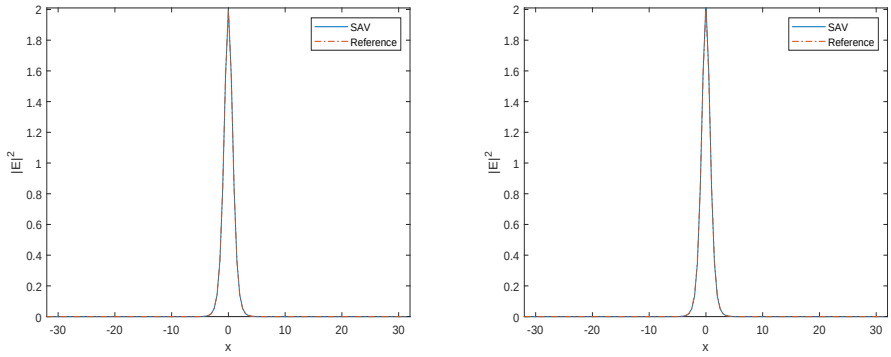

(c) $\epsilon = 0.125/256, dt = 10^{-3}$ (d) $\epsilon = 0.125/256, dt = 10^{-1}$

FIGURE 4.1. Numerical solutions of the electric field $|E(x,t)|^2$ at T=1.

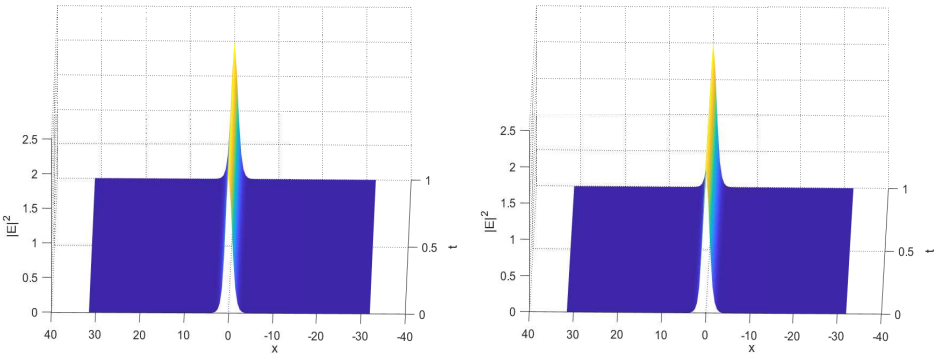

(a) $\epsilon = 0.125/256, dt = 10^{-3}$ (b) $\epsilon = 0.125/256, dt = 10^{-1}$

FIGURE 4.2. Numerical solutions of the electric field $|E(x,t)|^2$ at $[0,1]$.

Case III. The standard ZS with a plane-wave solution. Let $\Omega = [0, 2\pi)$ with $a = 0$ and $b = 2\pi$, we consider (1.1) with $\epsilon = 1$, $\alpha = 1$, $\lambda = 0$ and $\nu = -1$ with the

initial condition

$$E(x,0) = e^{i7x}, \quad N(x,0) = 1, \quad \partial_t N(x,0) = 0. \tag{4.3}$$

The problem (1.1) with the initial condition (4.3) admits a plane-wave solution [11]. We use the Fourier-spectral SAV scheme with the time step $dt = 10^{-5}$ and 256 Fourier modes. In Figure (4.3), we plot the numerical solution and the reference solution at $T = 2$ and $T = 4$, and we observe that our scheme provides very accurate solution for this test problem.

4.2. **Two-dimensional GZS with a linear damping term.** Mathematically, the GZS will blow up at finite time when $H^{GZS} < 0$. For fixed $E(\mathbf{x}, 0)$ and $N(\mathbf{x}, 0) = \nu|E(\mathbf{x}, 0)|^2$, there are three typical cases such that $H^{GZS} < 0$ [4]: (i) $\alpha = 1$, $\lambda \gg 1$, $\epsilon = O(1)$, $\nu = -1$; (ii) $\alpha \gg 1$, $\lambda = 0$, $\epsilon = O(1)$, $\nu = -1$; (iii) $\alpha = 1$, $\lambda = 0$, $0 < \epsilon \ll 1$, $\nu \ll -1$.

We choose $d = 2$ and present computations of the GZS with a linear damping term for the following cases:

$$\begin{gathered}\text{Case 1. } \alpha = 1,\ \lambda = 20,\ \epsilon = 1,\ \nu = -1,\\ \text{Case 2. } \alpha = 20,\ \lambda = 0,\ \epsilon = 1,\ \nu = -1,\\ \text{Case 3. } \alpha = 1,\ \lambda = 0,\ \epsilon = 0.1,\ \nu = -20,\end{gathered}$$

with the initial condition

$$E(x,y,0) = \frac{1}{\sqrt{\pi}} e^{-\frac{x^2+y^2}{2}}, \quad N(x,y,0) = \frac{\nu}{\pi} e^{-(x^2+y^2)}, \quad \partial_t N(x,y,0) = 0. \tag{4.4}$$

We solve the problem with the time step $dt = 10^{-3}$ and 256 Fourier modes on $\Omega = (-4,4)^2$ for Cases 1 and 2, and $\Omega = (-10,10)^2$ for Case 3. Since the solution is expected to blowup when λ becomes sufficiently large, we choose $C_0 = 7 \times 10^6$ so that we can simulate the blowup process during which the Hamiltonian may approach negative infinity. The simulation of the surface-plots of the electron density $|E(x,y,t)|^2$, and ion density fluctuation $N(x,y,t)$ for Case 1 at different λ are demonstrated in Figs. 4.4, 4.5 and 4.6 with $(\gamma, \Lambda) = (0.8, 20)$, $(0.1, 20)$, $(0.1, 100)$ respectively. We observe that no blowup occurs with $(\gamma, \Lambda) = (0.8, 20)$, but when we decrease γ to 0.1 while keeping other parameters to be the same, we observe clearly the blowup process in Figs. 4.5. Now, keeping $\gamma = 0.1$ while increasing λ to 100, we observe in 4.6 that the time to blowup is shorter with larger Λ.

Similar results are obtained for Cases 2 and 3, so for the sake of brevity, we do not report them here.

4.3. **Soliton-soliton collisions in one-dimensional GZS.** It is well known that the GZS admits the one-soliton solution [10, 9]:

$$\begin{aligned} E_s(x,t;\eta,V,\epsilon,\nu) &= \left[\frac{\lambda}{2} + \frac{\nu}{\epsilon^2}\left(\frac{1}{\epsilon^2} - V^2\right)^{-1}\right]^{-1/2} U_s(x,t;\eta,V,\epsilon,\nu),\\ N_s(x,t;\eta,V,\epsilon,\nu) &= \frac{\nu}{\epsilon^2}\left(\frac{1}{\epsilon^2} - V^2\right)^{-1} |E_s(x,t;\eta,V,\epsilon,\nu)|^2, \end{aligned} \tag{4.5}$$

where η and V are the amplitudes, and

$$U_s(x,t;\eta,V,\epsilon,\nu) = 2i\eta\,\mathrm{sech}[2\eta(x - Vt)] \exp\left[\frac{iVx}{2} + i\left(\frac{4\eta^2 - V^2}{4}\right)t\right].$$

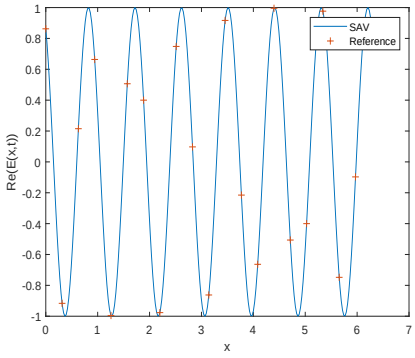

(a) $Re(E(x,t))$: real part of E

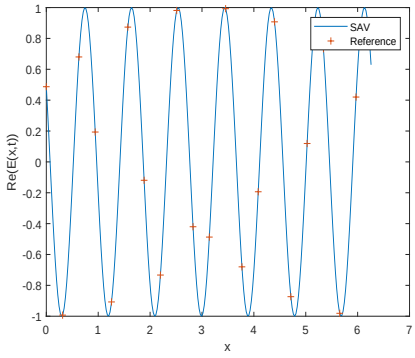

(b) $Re(E(x,t))$: real part of E

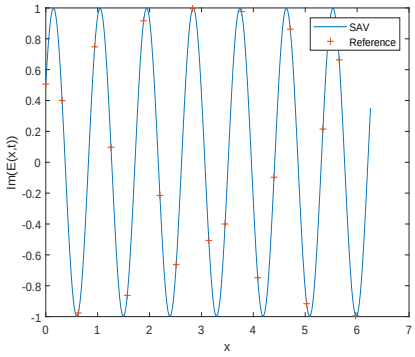

(c) $Im(E(x,t))$: imaginary part of E

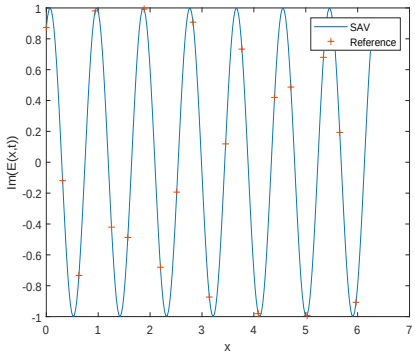

(d) $Im(E(x,t))$: imaginary part of E

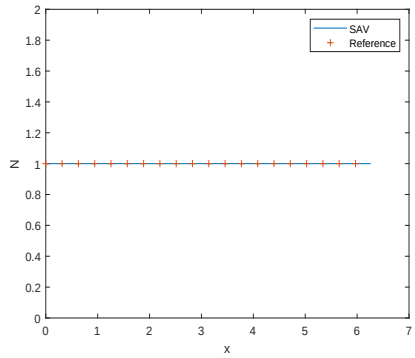

(e) $N(x,t)$

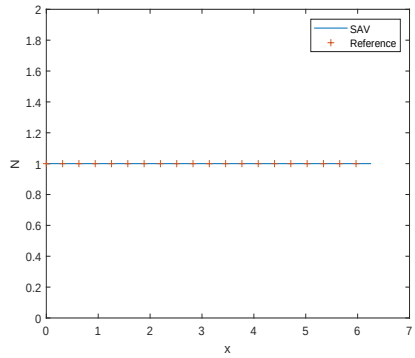

(f) $N(x,t)$

FIGURE 4.3. Numerical and reference solutions for Case III at T=2 (left column) and T=4 (right column).

We choose the initial conditions to be:

$$\begin{aligned} E(x,0) &= E_s(x+p,0;\eta_1,V_1,\epsilon,\nu) + E_s(x-p,0;\eta_2,V_2,\epsilon,\nu),\\ N(x,0) &= N_s(x+p,0;\eta_1,V_1,\epsilon,\nu) + N_s(x-p,0;\eta_2,V_2,\epsilon,\nu),\\ \partial_t N(x,0) &= \partial_t N_s(x+p,0;\eta_1,V_1,\epsilon,\nu) + \partial_t N_s(x-p,0;\eta_2,V_2,\epsilon,\nu), \end{aligned} \tag{4.6}$$

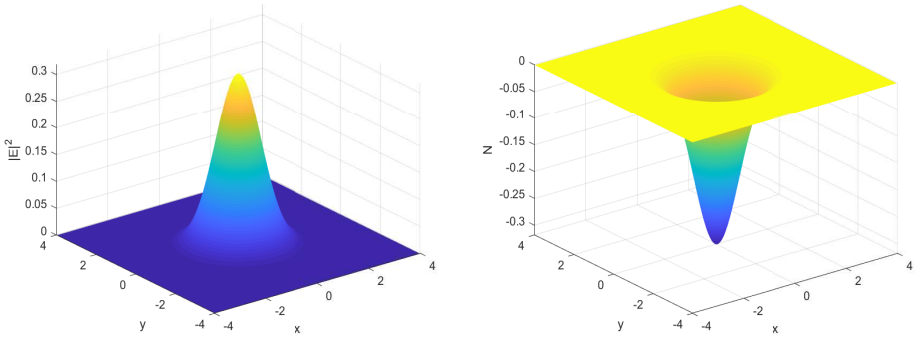

(a) $t = 0$ (b) $t = 0$

(c) $t = 0.5$ (d) $t = 0.5$

(e) $t = 1.0$ (f) $t = 1.0$

FIGURE 4.4. Numerical solutions in (4.2): surface-plots of the electron density $|E(x, y, t)|^2$ (left) and ion density fluctuation $N(x, y, t)$ (right) for Case 1 with $\gamma = 0.8$ and $\lambda = 20$.

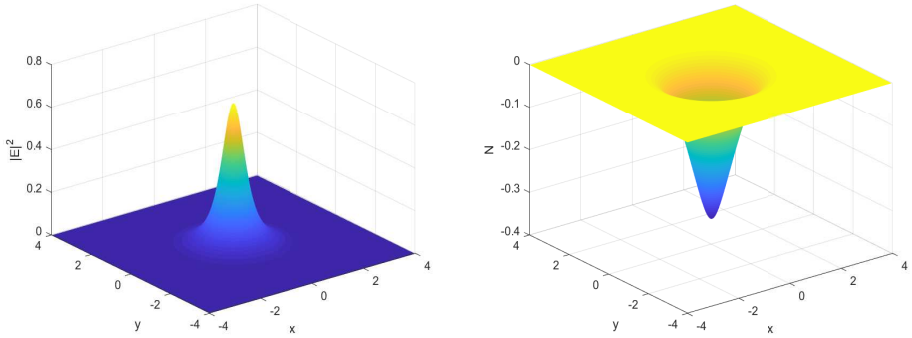

(a) t=0.2 (b) t=0.2

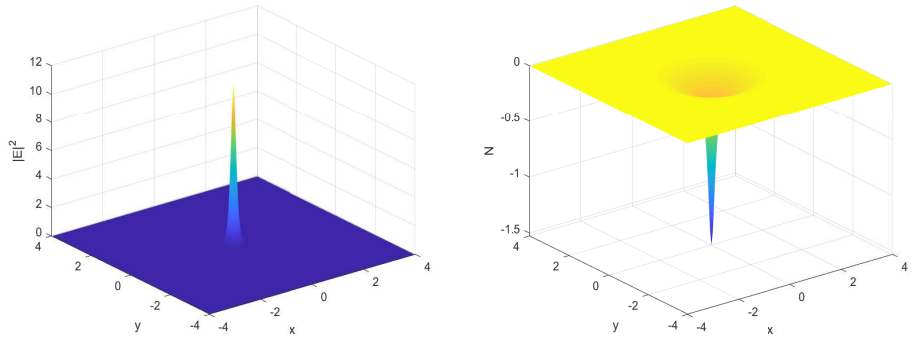

(c) t=0.39 (d) t=0.39

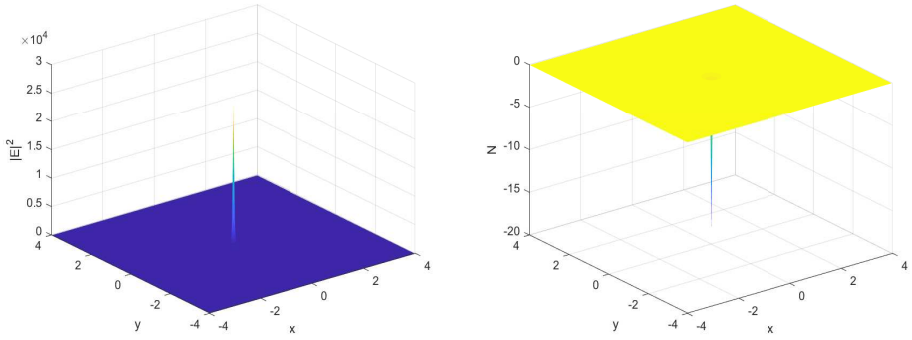

(e) t=0.406 (f) t=0.406

FIGURE 4.5. Numerical solutions in (4.2): surface-plots of the electron density $|E(x, y, t)|^2$ (left) and ion density fluctuation $N(x, y, t)$ (left) with $\gamma = 0.1$ and $\lambda = 20$.

where $x = \mp p$ are initial locations of the two solitons. The parameters are $\epsilon = 1$, $\lambda = 2$, $\gamma = 0$ and $p = 10$.

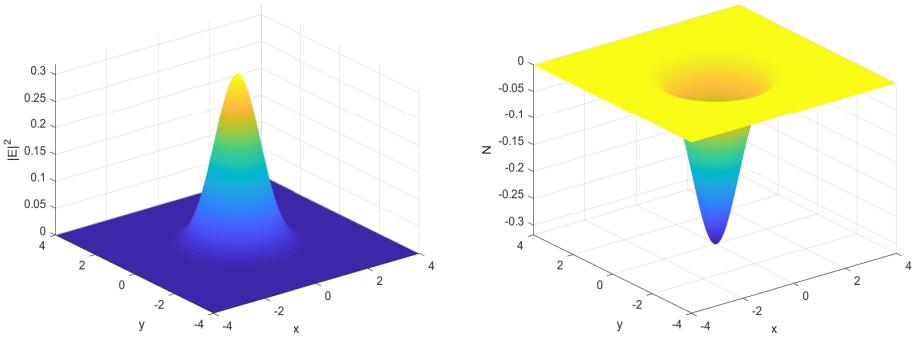

(a) $t = 0.02$ (b) $t = 0.02$

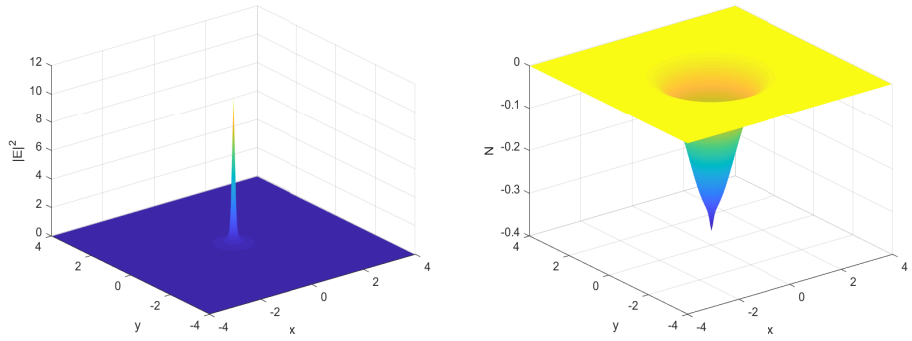

(c) $t = 0.09$ (d) $t = 0.09$

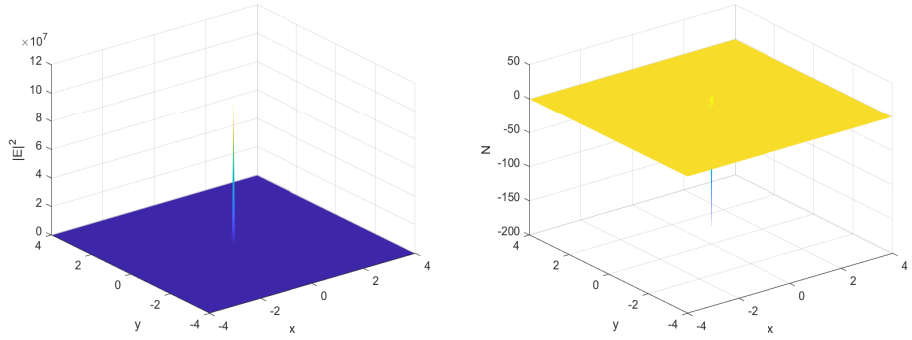

(e) $t = 0.094$ (f) $t = 0.094$

FIGURE 4.6. Numerical solutions in (4.2): surface-plots of the electron density $|E(x, y, t)|^2$ (left) and ion density fluctuation $N(x, y, t)$ (left) for Case 1 with $\gamma = 0.1$ and $\lambda = 100$.

In the following we shall simulate symmetric collisions, i.e., the collisions of solitons with equal amplitudes $\eta_1 = \eta_2 = \eta$ and opposite velocities $V_1 = -V_2 = V$, at subsonic velocities: $V < \frac{1}{\epsilon} = 1$. The following cases will be considered.

Case I. $\nu = 0.2,\ \eta = 0.3,\ \lambda = 2$ and $V = 0.5$;
Case II. $\nu = 2,\ \eta = 0.3,\ \lambda = 2$ and $V = 0.045$;
Case III. $\nu = 2,\ \eta = 0.3,\ \lambda = 2$ and $V = 0.45$.

We set $\Omega = (-25, 25)$, and use 128 Fourier modes and $dt = 10^{-2}$.

In Figs. 4.7, we plot **Case I** and observe an elastic soliton-soliton collision similar to those found in the nonlinear Schrödinger equation (NLS).

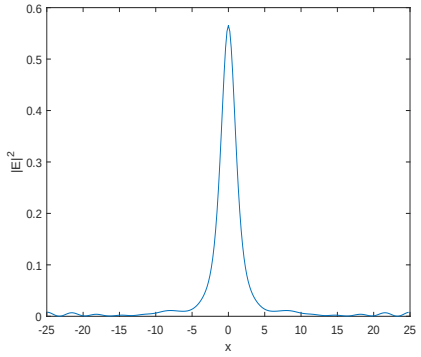

(a) Wave field $|E(x,t)|^2$ at final time T=31.8

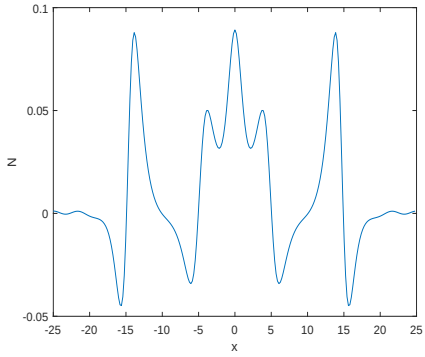

(b) Acoustic field $N(x,t)$ at final time T=31.8

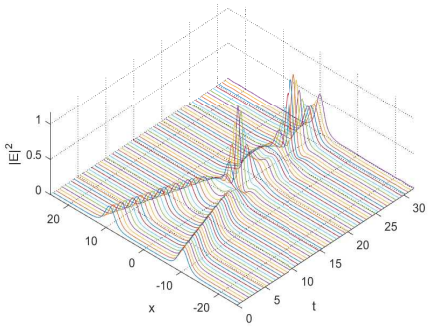

(c) Evolution of the wave field $|E(x,t)|^2$

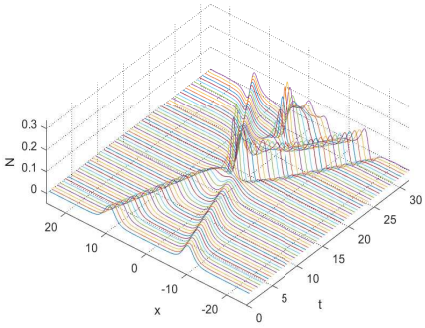

(d) Evolution of the acoustic field N

FIGURE 4.7. Numerical solutions in (4.3) for **Case I** with $\lambda = 2$.

We plot **Case II** in Fig. 4.8 and observe that the soliton collisions produce a new state with amplitude and width almost constant in time.

We plot **Case III** in Fig. 4.9. With an increased V as compared to **Case II**, the amplitude and size of the new state after collision show irregular oscillation along with acoustic sound waves. A simulation of **Case III** with $\lambda = 100$ is plotted in Fig. 4.10.

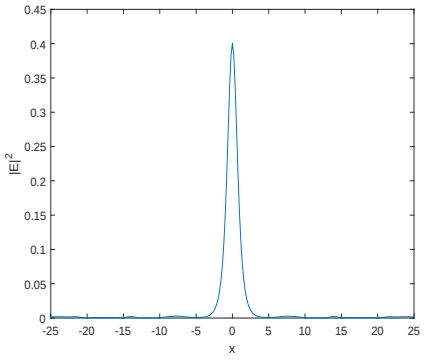

(a) Wave field $|E(x,t)|^2$ at final time T=200

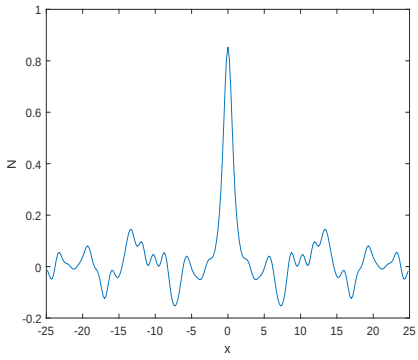

(b) Acoustic field $N(x,t)$ at final time T=200

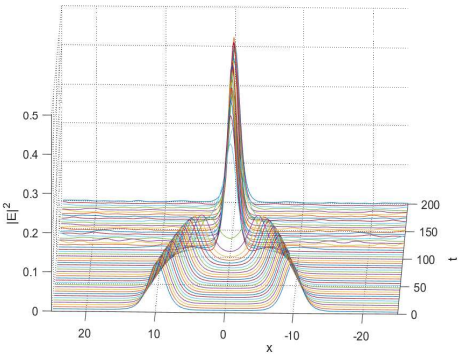

(c) Evolution of the wave field $|E(x,t)|^2$

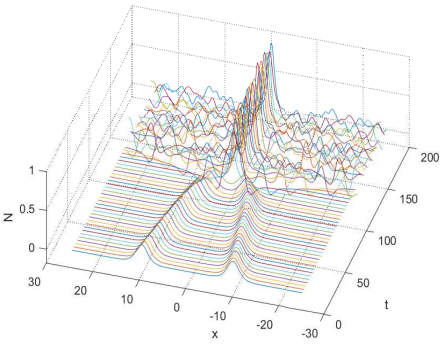

(d) Evolution of the acoustic field N

FIGURE 4.8. Numerical solutions in (4.3) for **Case II** with $\lambda = 2$.

4.4. **Dymanic simulation of three dimensional GVZS.** We consider the GVZS (1.4) in three dimension with the initial conditions

$$E_j(x,y,z,0) = e^{2i(\lambda_1 x-\lambda_2 y+2\lambda_3 z)}(\gamma_{1j}\gamma_{2j}\gamma_{3j})^{1/4}\frac{e^{-1/2(\gamma_{1j}x^2+\gamma_{2j}y^2++\gamma_{3j}z^2)}}{\sqrt{3}\pi^{3/4}}, j = 1,2,3$$
$$N(x,y,z,0) = e^{-2(x^2+y^2+z^2)}, \quad \partial_t N(x,y,z,0) = 0, \tag{4.7}$$

where (4.7), we take $\gamma_{11} = 1$, $\gamma_{21} = 2$, $\gamma_{31} = 4$; $\gamma_{12} = 4$, $\gamma_{22} = 2$, $\gamma_{32} = 1$; $\gamma_{13} = 2$, $\gamma_{23} = 4$, $\gamma_{33} = 1$. We choose the parameters in (1.4) to be $a = 2$, $\alpha = 1$, $\lambda = 0$, $\gamma = 0$, $\nu = -1$, $\epsilon = 1$, and consider the following two cases:

Case 1. Zero initial phase data, i.e.,$\lambda_1 = \lambda_2 = \lambda_3 = 0$.

Case 2. Nonzero initial phase data, i.e.,$\lambda_1 = \lambda_2 = \lambda_3 = 1$.

We take $\Omega = (-16,16)^3$, use 128^3 Fourier modes and $dt = 10^{-3}$. In Figure 4.11, we plot the evolution of the total wave energy $\|\mathbf{E}(t)\|^2$ and the wave energy of the three components of the electric field $\|E_1(t)\|^2$, $\|E_2(t)\|^2$ and $\|E_3(t)\|^2$ for **Case 1** and **Case 2**.

We observe from Figure 4.11 that the the total wave energy $\|\mathbf{E}(t)\|^2$ is well conserved in both cases.

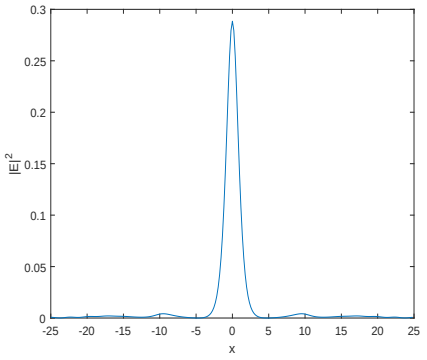

(a) Wave field $|E(x,t)|^2$ at final time T=30

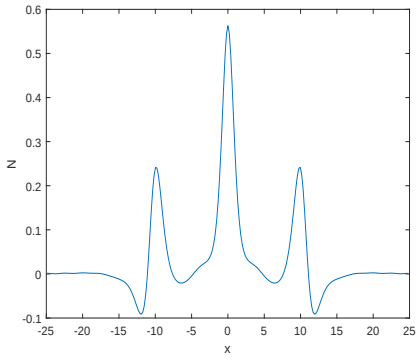

(b) Acoustic field $N(x,t)$ at final time T=30

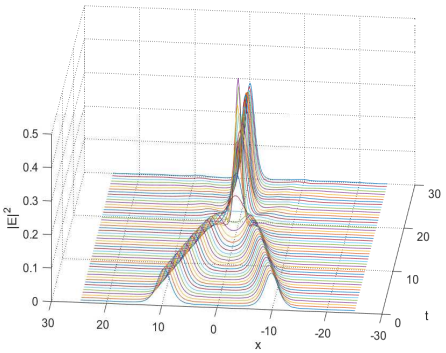

(c) Evolution of the wave field $|E(x,t)|^2$

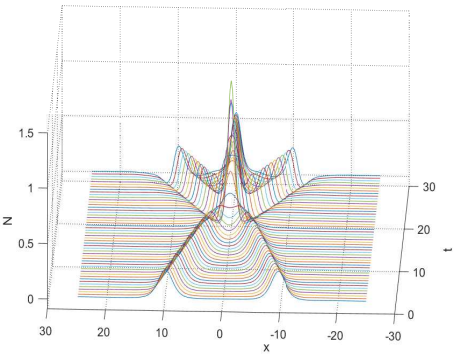

(d) Evolution of the acoustic field N

FIGURE 4.9. Numerical solutions in (4.3) for **Case III** with $\lambda = 2$.

In **Case 1**, the wave energy of the first components increases while the wave energy of the second component decreases so that the total wave energy is conserved. In **Case 2**, the first and the third components form essentially the same pattern but with opposite sign so that the total wave energy is conserved. The wave energy fluctuation is more pronounced than in **Case 1**.

5. **Concluding remarks.** The Scalar Auxiliary Variable (SAV) approach has been shown to be very effective for dissipative gradient flows. In this paper, we applied the SAV approach to construct efficient and accurate numerical schemes for the generalized Zakharov system (GZS) and generalized vector Zakharov system (GVZS), which are Hamiltonian systems. The Crank-Nicolson SAV schemes for these Hamiltonian systems enjoy all the advantages of the SAV approach for dissipative gradient flows, such as linear, unconditionally stable and only requiring solving decoupled linear system with constant coefficients at each time step, and furthermore, it conserves exactly a modified Hamiltonian, and conserve the wave energy and the original Hamiltonian with third-order accuracy and the momentum with second-order accuracy.

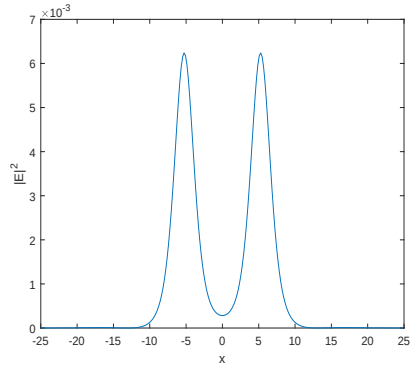

(a) Wave field $|E(x,t)|^2$ at final time T=30

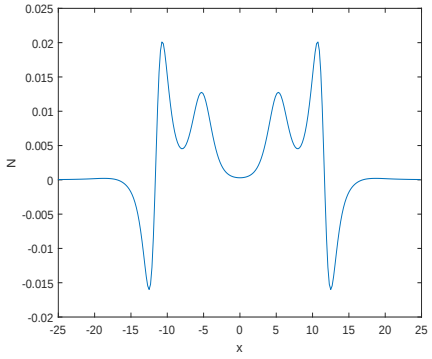

(b) Acoustic field $N(x,t)$ at final time T=30

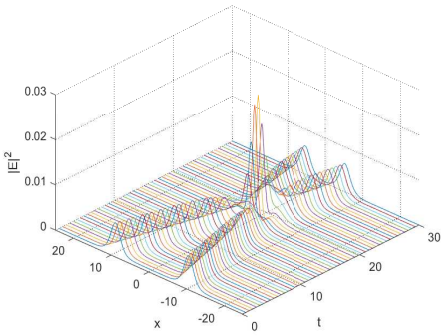

(c) Evolution of the wave field $|E(x,t)|^2$

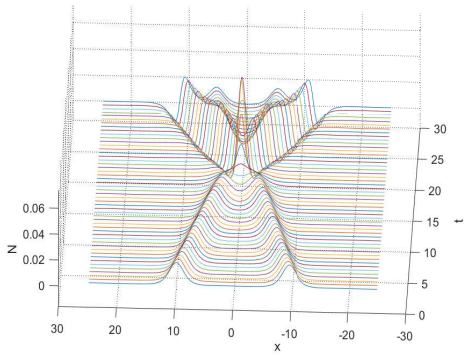

(d) Evolution of the acoustic field N

FIGURE 4.10. Numerical solutions in (4.3) for **Case III** with $\lambda = 100$.

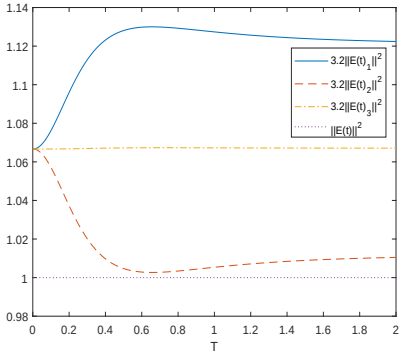

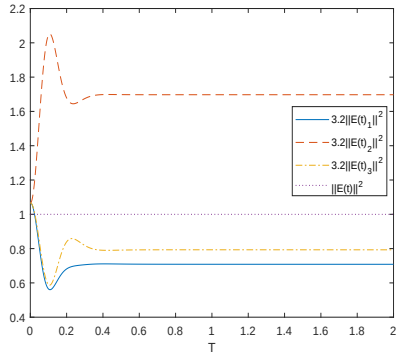

FIGURE 4.11. Evolution of the total wave energy $\|\mathbf{E}(t)\|^2$ and the wave energy of the three components of the electric field $\|E_1(t)\|^2$, $\|E_2(t)\|^2$ and $\|E_3(t)\|^2$ in (4.4) for **Case 1** (left) and **Case 2** (right).

We presented ample numerical results to validate the stability and accuracy and robustness of the schemes. The results presented in this paper indicate that the SAV approach is also very effective for Hamiltonian systems.

REFERENCES

[1] K. Amaratunga, J. R. Williams, S. Qian and J. Weiss, Wavelet–galerkin solutions for one-dimensional partial differential equations, *International Journal for Numerical Methods in Engineering*, **37** (1994), 2703–2716.

[2] X. Antoine, J. Shen and Q. Tang, An explicit scalar auxiliary variable pseudospectral scheme for the dynamics of nonlinear schrödinger and gross-pitaevskii equations, Preprint.

[3] W. Bao and C. Su, A uniformly and optimally accurate method for the zakharov system in the subsonic limit regime, *SIAM Journal on Scientific Computing*, **40** (2018), A929–A953.

[4] W. Bao and F. Sun, Efficient and stable numerical methods for the generalized and vector zakharov system, *SIAM Journal on Scientific Computing*, **26** (2005), 1057–1088.

[5] J. P. Boyd, *Chebyshev and Fourier Spectral Methods*, Courier Corporation, 2001.

[6] W. Cai, C. Jiang, Y. Wang and Y. Song, Structure-preserving algorithms for the two-dimensional sine-gordon equation with neumann boundary conditions, *Journal of Computational Physics*, **395** (2019), 166–185.

[7] Q. Chang and H. Jiang, A conservative difference scheme for the zakharov equations, *Journal of Computational Physics*, **113** (1994), 309–319.

[8] R. T. Glassey, Convergence of an energy-preserving scheme for the zakharov equations in one space dimension, *Mathematics of Computation*, **58** (1992), 83–102.

[9] H. Hadouaj, B. A. Malomed and G. A. Maugin, Dynamics of a soliton in a generalized zakharov system with dissipation, *Physical Review A*, **44** (1991), 3925–3931.

[10] H. Hadouaj, B. A. Malomed and G. A. Maugin, Soliton-soliton collisions in a generalized zakharov system, *Physical Review A*, **44** (1991), 3932–3940.

[11] P. K. Newton, Wave interactions in the singular zakharov system, *Journal of Mathematical Physics*, **32** (1991), 431–440.

[12] G. L. Payne, D. R. Nicholson and R. M. Downie, Numerical solution of the zakharov equations, *Journal of Computational Physics*, **50** (1983), 482–498.

[13] B. F. Sanders, N. D. Katopodes and J. P. Boyd, Spectral modeling of nonlinear dispersive waves, *Journal of Hydraulic Engineering*, **124** (1998), 2–12.

[14] J. Shen, T. Tang and L.-L. Wang, *Spectral Methods: Algorithms, Analysis and Applications*, volume 41, Springer Science & Business Media, 2011.

[15] J. Shen, J. Xu and J. Yang, The scalar auxiliary variable (sav) approach for gradient flows, *Journal of Computational Physics*, **353** (2018), 407–416.

[16] J. Shen, J. Xu and J. Yang, A new class of efficient and robust energy stable schemes for gradient flows, *SIAM Review*, **61** (2019), 474–506.

[17] C. Sulem and P. L. Sulem, Regularity properties for the equations of langmuir turbulence, *Comptes Rendus Hebdomadaires Des Seances De L Academie Des Sciences Serie A*, **289** (1979), 173–176.

[18] G. W. Wei, Discrete singular convolution for the solution of the fokker–planck equation, *The Journal of Chemical Physics*, **110** (1999), 8930–8942.

[19] V. E. Zakharov et al., Collapse of langmuir waves, *Sov. Phys. JETP*, **35** (1972), 908–914.

Received March 2020; revised July 2020.

E-mail address: shen7@purdue.edu
E-mail address: znan2017@163.com